

SAND REPORT

SAND2003-0845

Unlimited Release

Printed March 2003

Photonic Crystals for Enhancing Thermophotovoltaic Energy Conversion

Shawn Lin, J.G. Fleming, J. Moreno

Prepared by
Sandia National Laboratories
Albuquerque, New Mexico 87185 and Livermore, California 94550

Sandia is a multiprogram laboratory operated by Sandia Corporation,
a Lockheed Martin Company, for the United States Department of Energy's
National Nuclear Security Administration under Contract DE-AC04-94-AL85000.

Approved for public release; further dissemination unlimited.



Sandia National Laboratories

Issued by Sandia National Laboratories, operated for the United States Department of Energy by Sandia Corporation.

NOTICE: This report was prepared as an account of work sponsored by an agency of the United States Government. Neither the United States Government, nor any agency thereof, nor any of their employees, nor any of their contractors, subcontractors, or their employees, make any warranty, express or implied, or assume any legal liability or responsibility for the accuracy, completeness, or usefulness of any information, apparatus, product, or process disclosed, or represent that its use would not infringe privately owned rights. Reference herein to any specific commercial product, process, or service by trade name, trademark, manufacturer, or otherwise, does not necessarily constitute or imply its endorsement, recommendation, or favoring by the United States Government, any agency thereof, or any of their contractors or subcontractors. The views and opinions expressed herein do not necessarily state or reflect those of the United States Government, any agency thereof, or any of their contractors.

Printed in the United States of America. This report has been reproduced directly from the best available copy.

Available to DOE and DOE contractors from

U.S. Department of Energy
Office of Scientific and Technical Information
P.O. Box 62
Oak Ridge, TN 37831

Telephone: (865)576-8401
Facsimile: (865)576-5728
E-Mail: reports@adonis.osti.gov
Online ordering: <http://www.doe.gov/bridge>

Available to the public from

U.S. Department of Commerce
National Technical Information Service
5285 Port Royal Rd
Springfield, VA 22161

Telephone: (800)553-6847
Facsimile: (703)605-6900
E-Mail: orders@ntis.fedworld.gov
Online order: <http://www.ntis.gov/help/ordermethods.asp?loc=7-4-0#online>



Photonic Crystals for Enhancing Thermophotovoltaic Energy Conversion

Shawn Lin
Photonic Research Department

J.G. Fleming
MEMS and Novel Si Science and Technology

J. Moreno
Thermal Solar Technology

Sandia National Laboratories
P.O. Box 5800
Albuquerque, NM 87185-0603

ABSTRACT

Thermophotovoltaics (TPV) converts the radiant energy of a thermal source into electrical energy using photovoltaic cells. TPV has a number of attractive features, including: fuel versatility (nuclear, fossil, solar, etc.), quiet operation, low maintenance, low emissions, light weight, high power density, modularity, and possibility for cogeneration of heat and electricity. Some of these features are highly attractive for military applications (Navy and Army). TPV could also be used for distributed power and automotive applications wherever fuel cells, microturbines, or cogeneration are presently being considered if the efficiencies could be raised to around 30%.

This proposal primarily examine approaches to improving the radiative efficiency. The ideal irradiance for the PV cell is monochromatic illumination at the bandgap. The photonic crystal approach allows for the tailoring of thermal emission spectral bandwidth

at specific wavelengths of interest. The experimental realization of metallic photonic crystal structures, the optical transmission, reflection and absorption characterization of it have all been carried out in detail and will be presented next. Additionally, comprehensive models of TPV conversion has been developed and applied to the metallic photonic crystal system.

INTRODUCTION

We propose to examine photonic crystals and advanced optical structures to substantially improve the radiative efficiency in TPV. Photonic lattices use a periodic modulation of the refractive index to alter the photonic density-of-states spectrum. Photonic lattices can alter the radiative spectrum and angular distribution of a radiator, or it can be used as an optical filter with a potentially 180° acceptance angle for a 3D photonic lattice (“photonic crystal”). (Control of the angular distribution is important for minimizing the radiative losses in the TPV cavity.)

Sandia is a leader in photonic crystals due to our leadership in MEMS technology. As an example, Sandia demonstrated the first 3D photonic crystal in the IR range using silicon MEMS technology (Fig. 1). These crystals were also used to demonstrate the alteration of spectral exitance by a photonic structure that could be so useful for TPV (Fig. 2). Finally, we have demonstrated photonic crystals with an intentionally introduced defect (microcavity) that can be the ideal passband optical filter for TPV.

The accomplishments of this LDRD funded project are described below.

Chapter 1

All Metallic, Absolute Photonic Band Gap Three-dimensional Photonic-Crystals for Energy Applications

We point out a new direction in photonic crystal research that involves the interplay of photonic band gap (PBG) rejection [1-3] and photonic band edge absorption. It is proposed that an absolute PBG may be used to frustrate infrared part of Black-body emission and, at the same time, its energy is preferentially emitted through a sharp absorption band. Potential application of this new PBG mechanism includes highly efficient incandescent lamps and enhanced thermophotovoltaic energy conversion [4]. Here, a new method is proposed and implemented to create an all-metallic 3D crystal at infrared wavelengths, λ , for this purpose. Superior optical properties are demonstrated. The use of metal leads to the opening of a large and absolute photonic band gap (from $\lambda \sim 8\mu\text{m}$ to $> 20\mu\text{m}$). The measured attenuation strength of ~ 30 dB/ per unit cell at $\lambda = 12\mu\text{m}$ is the strongest ever reported for any 3D crystals at infrared λ . At the photonic band edge, the speed-of-light is shown to slow down considerably and an order-of-magnitude absorption enhancement observed. In the photonic allowed band, $\lambda \sim 5\mu\text{m}$, the periodic metallic-air boundaries mold the flow of light, leading to an extraordinarily large transmission enhancement. The realization of 3D absolute band-gap metallic photonic crystal will pave the way for highly efficiency energy applications and for combining and integrating different photonic transport phenomena in a photonic crystal.

It is known that a 3D metallic photonic crystal is promising for obtaining a larger photonic band gap [5-7], for achieving new EM phenomenon [8-10] and for high temperature ($>1,000\text{C}$) applications. However, metals offer theoretical challenges in the investigation of photonic band gap behavior especially in the infrared (IR) and optical wavelength, as they are often dispersive and absorptive [11]. The difficulties in fabricating 3D metallic crystal in the IR and optical wavelengths present another challenge. So far, studies of metallic photonic crystals are mostly concentrated at microwave and millimeter wavelengths [9, 12-13]. One exception is work done by McIntosh et al on infrared metallodielectric photonic crystals [7]. Also, fabrication of optical metallic 3D crystal using self-assembly method is just emerging [14,15].

In this work, fabrication of a Tungsten 3D photonic crystal was realized using a newly proposed method. It is done by selectively removing Si from already fabricated polysilicon/SiO₂ structures, and back filling the resulting mold with chemical vapor deposited (CVD) Tungsten. This method can be extended to create almost any 3D single-crystal metallic photonic crystals at infrared λ , which are previously not achievable by any other means. A SEM image of the fabricated four-layer 3D Tungsten photonic crystal is shown in Fig.1 (a) and (b).

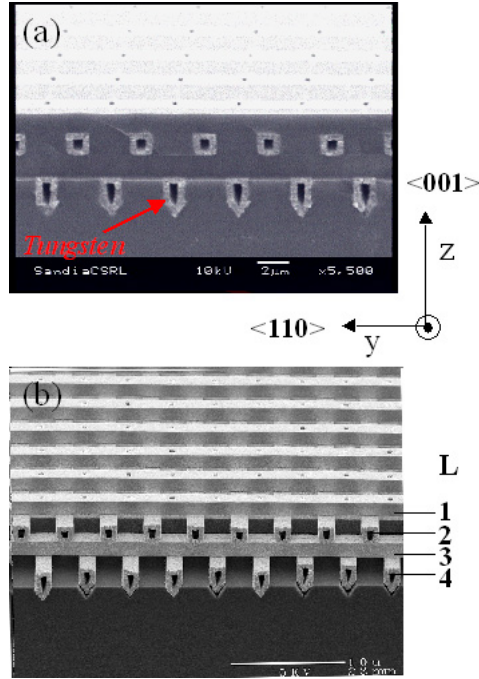


Figure 1

The optical properties of the 3D Tungsten photonic crystal are characterized using a Fourier-transform infrared measurement system for wavelengths ranging from $\lambda = 1.5$ to $25 \mu\text{m}$ [16]. To obtain reflectance (R), a sample spectrum was taken from a 3D Tungsten crystal first and then normalized to a reference spectrum of a uniform silver mirror. To find the absolute transmittance (T), a transmission spectrum taken from a 3D Tungsten crystal sample was normalized to that of a bare silicon wafer. This normalization procedure is intended to calibrate away extrinsic effects, such as light reflection at the air-silicon interface and silicon absorption. For tilt-angle transmission measurements, the sample is mounted onto a rotational stage with a rotational angles spanned from $\theta=0^\circ$ to 60° , measured from the surface normal, i.e. $\langle 001 \rangle$ direction.

The absolute reflectance (black diamonds) and transmittance (blue circles) of a four-layer 3D Tungsten photonic-crystal is shown in Fig.2(a). Light propagates along the $\langle 001 \rangle$ direction of the crystal and is un-polarized. The reflectance exhibits oscillations at $\lambda < 5.5 \mu\text{m}$, raises sharply at $\lambda \sim 6 \mu\text{m}$ (the band edge) and finally reaches a high reflectance of 90% for $\lambda > 8 \mu\text{m}$. Correspondingly, the transmittance shows distinct peaks at $\lambda < 5.5 \mu\text{m}$, decreases sharply at $\lambda \sim 6 \mu\text{m}$ (the photonic band edge) and then vanishes to below 1% for $\lambda > 8 \mu\text{m}$. The dashed line is for reference purpose and is a transmittance taken from a 6000\AA uniform Tungsten film. The simultaneous high R and low T at $\lambda > 8 \mu\text{m}$ is indicative of the existence of a photonic band gap in the Tungsten 3D photonic

crystal. The attenuation is as large as $\sim 30\text{dB}$ at $\lambda=10\ \mu\text{m}$ for our 4-layer sample, or equivalently a unit cell. The multiple oscillations at $\lambda < 5.5\ \mu\text{m}$ are attributed to photonic density-of-states (DOS) oscillations in the photonic allowed band.

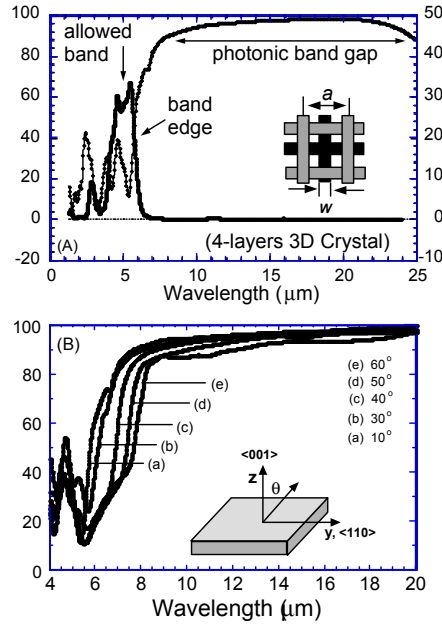


Figure 2

To confirm our experimental observation, a transfer-matrix calculation [5] of transmittance and reflectance is carried out and the results shown in Fig.3. The structure parameters used are the same as the fabricated structure other than it has a slightly higher filling fraction, 33.3%. A frequency dependent dielectric functions $\epsilon_1(\omega)$, $\epsilon_2(\omega)$ for Tungsten were also used to take into account the dispersion and absorption effects [17, 18].

Fig.3(a) shows the computed result for a 4-layer ($N=4$) 3D crystal, which correctly predicts photonic band edge position and the gap size. More importantly, the transmittance (blue color curve) also shows a high transmission at $\lambda \sim 5\ \mu\text{m}$. Although, the computed peak value (80%) is about three-times higher and the full-width-half-maximum ($\sim 0.5\ \mu\text{m}$) three times narrower than the measured one. By increasing N to 6 (i.e. a sample thickness of $9.6\ \mu\text{m}$), the peak transmission reaches a stable value of 95%, further confirming the notion of a photonic crystal. Surprisingly, there exists a sharp absorption peak (red color spectrum) at $\lambda \sim 6-7\ \mu\text{m}$. The peak λ is near the band edge and its absorptance is $\sim 50\%$. Using a photoacoustic spectroscopy technique [19], a direct absorption measurement is performed and a clear absorption peak of 22% is observed at $\lambda \sim 6\ \mu\text{m}$. For comparison, the absorptance for a uniform Tungsten-film at this λ is measured to be $\sim 1\%$. For $\lambda < 4.5\ \mu\text{m}$, computed reflectance ($>75\%$) is much higher than

the observed one (20-30%). Since metallic absorption loss is not important in this λ -range [17], the observed low R is attributed to scattering losses. One source of scattering is structure imperfections such as the keyholes shown in Fig.1.

The photonic band gap attenuation in a 3D metallic photonic crystal must not be confused with typical metallic attenuation. To illustrate this point, transmission spectra for 3D crystals of different number-of-layers, $N=2, 4$ and 6 , were computed and the results shown in Fig. 3(b). The dashed line is a reference spectrum taken from a uniform 6000\AA Tungsten-film. Consistent with its small metallic skin-depth ($300\text{-}500\text{\AA}$ for $1\mu\text{m} < \lambda < 25\mu\text{m}$), the Tungsten-film transmittance is very low ($T < 10^{-8}$) and is nearly λ -independent. The sample spectrum, on the other hand, exhibits a much higher transmission ($T \sim 10^{-1}$) for $\lambda < 6\mu\text{m}$, suggesting that photonic transport in this spectral range is not dominated by metallic attenuation. Moreover, a strong λ -independent and N -dependent is observed in the band gap regime ($\lambda > 8\mu\text{m}$). This N -dependence indicates that transmittance attenuation at $\lambda > 8\mu\text{m}$ scales with layer-thickness of our 3D structure, but not the metallic skin depth. Thus, the attenuation at $\lambda > 8\mu\text{m}$ is due primarily to photonic band gap effect. The attenuation constant in the photonic band gap is very large. It is $\sim 32, 56$ and 64 dB per unit cell at $\lambda = 10, 20$ and $40\mu\text{m}$, respectively. This means that as few as one unit cell of a 3D Tungsten crystal is sufficient for achieving strong electromagnetic waves attenuation.

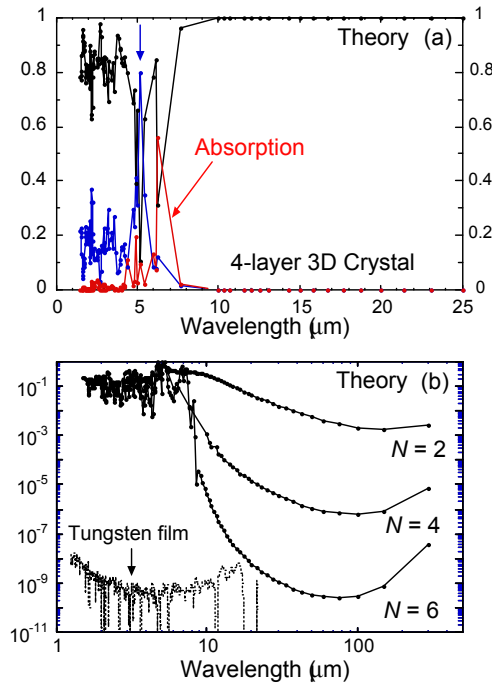


Figure 3

To prove the existence of absolute metallic photonic band-gap, i.e. a common band gap for light propagating in all directions, a tilt-angle reflection experiment was

conducted. Five tilt-angle spectra were shown in Fig.2(b) for $\theta = 10, 30, 40, 50$ and 60° , respectively. As θ is increased, the band edge position moves from $\lambda \sim 6\mu\text{m}$ for $\theta = 10^\circ$ to $\lambda \sim 8\mu\text{m}$ for $\theta = 60^\circ$. Nonetheless, both the oscillating features at $\lambda < 6\mu\text{m}$ and the high reflectance at longer wavelength remain for all θ s. Despite the shift in band edge, a large complete photonic band-gap exists, from $\lambda \sim 8\mu\text{m}$ to $\lambda > 20\mu\text{m}$, for our 3D Tungsten photonic crystal. Such an extraordinarily large band gap is ideally suited for suppressing broadband Blackbody radiation in the infrared [20] and re-cycling its energy into the visible spectrum. In the photon recycling process, an absolute 3D photonic band gap completely frustrates IR thermal emission and forces the radiation into a selective emission band. Consequently, energy is not wasted in heat generation, but rather been re-channeled into a useful emission band. According to Kirchoff's law, the integrated absorptance equals integrated emissivity [21]. The absorption peak near band edge (see Fig.3) is then an ideal channel for light emission. As a Tungsten 3D crystal can be heated up to an elevated temperature of $>1500\text{C}$, the emission band can be tailored to be in the visible, giving rise to a highly efficient incandescent lamp. This new phenomenon is based on a powerful interplay between photonic band gap rejection and photonic band edge enhanced absorption, which is made possible by the creation of a 3D metallic crystal. This photonic band gap mechanism for energy recycling has major energy consequences in thermal-photovoltaic (TPV) application as well [4]. Using our 3D structure as an emitter, a TPV model calculation [4] shows that the TPV conversion efficiency reaches 51%, which is to be compared to 12.6% efficiency for a Black-Body emitter.

A 3D metallic crystal not only exhibits a strong photonic band gap, but also possesses unique transmission and absorption characteristics. It is noted that while transmittance through a uniform 6000\AA Tungsten-film is extremely small $T < 10^{-8}$, peak transmission through 3D W-crystal sample at $\lambda \sim 5\mu\text{m}$ is high, $T \sim 25\text{-}30\%$. We may also approximate our 3D structure as arrays of sub-wavelength holes and the estimated transmission efficiency is also small, 3×10^{-5} [22]. Here, the hole-radius is estimated from the straight opening shown in the inset of fig-1a. None of the above two approximations can explain the observed transmission enhancement. A further transfer-matrix calculation reveals that the transmission peak λ scales linearly with lattice constant a and depends on material filling-fraction. A similar enhancement effect and scaling behavior have also been observed in 2D metallic thin film hole-arrays and was attributed to surface plasma excitation [23]. However, its peak λ is independent of the hole-diameter, or equivalently hole filling-fraction. The surface plasmon picture is useful in describing EM modes in thin films with small holes, where the film thickness is small compare with λ [23]. It is likely that plasmon effect will play a role. However, a formal theoretical classification of the nature of the EM modes in complex structures as ours would give better insights into this extraordinary phenomenon. Such EM modes must also manifest the 3D crystal symmetry and facilitate waveguiding through metallic openings [24]. To explore the manner by which light-wave manages to mold itself according to the intricate 3D metallic structure (and to the Bloch Theorem), a FDTD calculation is carried out.

FDTD Calculations are done for a six-layer 3D crystal sample at three different λ s ($\lambda=5.2, 6.5$ and $12\mu\text{m}$) and at two separate time steps T ($=1\Delta t=0.133 \times 10^{-12}$ second and

$2\Delta t$). This calculation assumes a perfect metallic boundary condition, as Tungsten material absorption is minimal in this λ s [17]. Here the Δt s are chosen to display the transient and steady state electromagnetic wave distribution, respectively. The color plot is expressed in a logarithmic scale and shows electric intensity profile in the y-z plane. The light source is a continuous wave point source, indicated by arrows, and is placed at mid-point of the first layer ($L=1$). The Tungsten rods show up as red regions. At $\lambda=5.2\ \mu\text{m}$ and $T=1\Delta t$, see Fig 4.(a), light-wave intensity (the dark blue color) diverges in y-direction and meanwhile its wave-front propagates along z-axis up to $L=6$. At $T=2\Delta t$, Fig. 4(b), light has transported uniformly through all six layers and its intensity reached a steady state. It is noted that, at the metallic boundaries, there exists a strong field gradient, from red, green to blue, encompassing the metallic rods. These periodic metallic-air boundaries mold the flow of light and dictate its Bloch-wave transport characteristics. At $\lambda=6.5\ \mu\text{m}$, Fig. 4(c) and (d), light also diverges in y-axis, propagates less intensively toward $L=4$ at $T=1\Delta t$ and eventually through $L=6$ at $T=2\Delta t$. Additionally, the speed-of-light is slow down considerably at this λ . The weaker transmission and the retarded speed-of-light are clear manifestation of light propagation at a photonic band edge. This retardation, along with percolation of light through the 3D structure, may be responsible for the large absorption at $\lambda=6-7\ \mu\text{m}$. Here, the very unique photonic band edge behavior leads to order-of-magnitudes absorption-enhancement. At $\lambda=12\ \mu\text{m}$ (see Fig.4 (e) and (f)), light does not transport through the six-layer structure and is totally reflected back, as it is in the photonic band gap region.

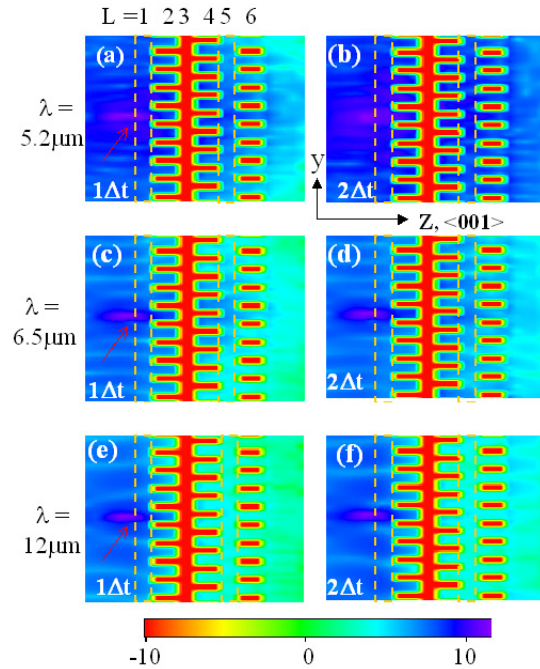


Fig.4

Finally, we address feasibility and challenges for realizing practical incandescent lamps. The first challenge involves the creation of metallic photonic crystals in the visible wavelengths. The minimum feature size needs to be made 10 times smaller, i.e. 100-200 nano-meter. Current commercially available optical lithographic steppers can produce feature size of 150-180nm over a 12-inch silicon wafer and down to 120nm by year 2002. These steppers are designed for large-scale production with high yields, which should help driving the production cost down. Another alternative is to use direct electron-beam write lithographic technique, although it is more costly. It is also noted that a photonic band gap is effective only when infrared light is emitted within the 3D photonic crystal. Emission from the sample surfaces would experience less photonic band gap effect. One solution is to passivate the surface layers. By applying a thin insulating surface coating, electrical current can only pass through bulk portion of the 3D crystal, and high emission efficiency is again achievable.

Methods for Creating 3D single-crystal metallic photonic crystal

Details on the fabrication of the polysilicon/SiO₂ 3D photonic crystal, which formed the basis of the Tungsten-molds, are given in reference-16. Briefly, the 3D silicon photonic crystal consists of layers of one-dimensional rods with a stacking sequence that repeats itself every four layers (a unit cell), and has a face-center-tetragonal lattice symmetry [25]. Further details on the rest of the processing steps are as follows. Firstly, the polysilicon in a 3D silicon photonic crystal was removed using a 6M, 85C KOH etch which has a selectivity of ~100:1. Over-etch during the KOH process, which is required to ensure the removal of all the poly-silicon, results in the formation of a “V” structure on the bottom of the layer contacting the substrate. This is due to etching of the underlying substrate. The KOH etch effectively stops when the etch-front encounters the slow etching {111} planes of the substrate, thus forming a “V” groove (see Fig.1). However this artifact does not appear to significantly impact photonic band gap performance. Secondly, the blanket CVD Tungsten film does not adhere to silicon dioxide and was therefore grown on a 50nm thick TiN adhesion layer deposited by reactive ion sputtering. The bulk of the Tungsten film was deposited at high pressure (90 Torr) from WF₆ and H₂. The chemical vapor deposition of Tungsten results in films of very high purity; the film resistivity was 10 microOhm-cm. The step coverage of the deposition process is not 100% and this gives rise to the formation of a keyhole in the center of the more deeply imbedded lines (see Fig.1b). However, the resulting thickness is far greater than the skin depth of Tungsten and the parts typically retain sufficient structural integrity to be handled readily. And lastly, excess Tungsten on the surface was removed by chemical mechanical polishing and the oxide mold was removed with a 1:1 HF solution, which etches SiO₂ but not Tungsten or TiN. All of the techniques employed throughout are modifications of standard CMOS processes and all work was performed on commercially available, monitor grade, six-inch silicon wafers.

References

1. Yablonovitch, E. Inhibited spontaneous emission in solid-state physics and electronics, *Phys. Rev. Lett.* **58**, 2059-2062 (1987).
2. John, S. Electromagnetic absorption in a disordered medium near a photon mobility edge, *Phys. Rev. Lett.* **53**, 2169-2172 (1984).
3. Genack, A. & Garcia, N. Observation of photon localization in a three-dimensional periodic array, *Phys. Rev. Lett.* **66**, 2063-2067 (1991).
4. Zenker, M. , Heinzl, M., Stollwerck, G., Ferber, J., and Luther, J., Efficiency and power density potential of combustion-driven thermophotovoltaic systems using GaSb photovoltaic cells, *IEEE Trans. Elec. Dev.* **48**, p. 367-376 (2001).
5. Sigalas, M.M., Chan, C.T., Ho, K.M. and Soulokous, C.M., Metallic photonic band-gap materials, *Phys. Rev.* **B52**, 11744-11751 (1995).
6. Fan, S., Villeneuve, P.R., and Joannopoulos, J.D., Large omnidirectional band gaps in metallodielectric photonic crystals, *Phys. Rev.* **B54**, 11245-11251 (1996).
7. McIntosh, K.A., et. al., Three-dimensional metallodielectric photonic crystals exhibiting resonant infrared stop bands, *Appl. Phys. Lett.* **70**, 2937-2939 (1997).
8. Sievenpiper, D.F., Sickmiller, M.E., and Yablonovitch, E., 3D wire mesh photonic crystals, *Phys. Rev. Letts.* **76**, 2480-2483 (1996).
9. Moroz, A., Three-dimensional complete photonic-band-gap structures in the visible, *Phys. Rev. Letts.* **83**, 5274-5277 (1999).
10. Pendry, J.B., Negative refraction makes a perfect lens, *Phys. Rev. Letts*, **85**, 3966-3969 (2000).
11. For a general reference, please see Handbook of Optical Constants of Solids, p. 275-409, edited by E.D. Palik, (Academic Press, San Diego, USA, 1998).
12. Ozbay, E., et. al., Defect structures in metallic photonic crystals, *Appl. Phys. Lett.* **69**, 3797-3799 (1996).

13. Sievenpiper, D.F., Yablonovitch, E., Winn, J.N., Fan, S., Villeneuve, P.R., and Joannopoulos, J.D., 3D metallo-dielectric photonic crystals with strong capacitive coupling between metallic islands, *Phys. Rev. Letts.* **80**, 2829-2832 (1998).
14. Velev, O.D., Kaler, E. W., Structured porous materials via colloidal crystal templating: from inorganic oxides to metals, *Adv. Mater.* **12**, 531-534 (2000).
15. Zakhidov, A.A., et. al., Three-dimensionally periodic conductive nanostructures: network versus cerment topologies for metallic PBG, *Synthetic Metals* **116**, 419-426 (2001).
16. Lin, S.Y., et. al., A three-dimensional photonic crystal in the infrared wavelengths, *Nature* **394**, 252-253 (1998).
17. M.A. Ordal, et al., Optical properties of the metals Al, Co, Cu, Au, Fe, Pb, Ni, Pd, Pt, Ag, Ti, and W in the infrared and far infrared, *Applied Optics* **22**, 1099-1119 (1983).
18. El-Kady, I., Sigalas, M.M., Biswas, R., Ho, K.M., and Soukoulis, C.M., Metallic photonic crystals at optical wavelengthsm *Phys. Rev. B* **62**,15299-15301 (2000).
19. McClelland, J.F., Jones, R.W., Lou, S., and Seaverson, L.M., A Practical guide to FTIR photoaccoustic spectroscopy, in *Practical sampling teciniques for infrared analysis*, P.B. Coleman, Ed. (CRC Press, Boca Raton, Florida, 1993), Chapter 5.
20. Lin, S.Y., Fleming, J.G., Chow, E., and Bur, J., Enhancement and suppression of thermal emission by a three-dimensional photonic crystal, *Phys. Rev. B* **62**, R2243, (2000).
21. “*Infrared Detectors and Systems*”, by E. L. Dereniak and G.D. Boreman, John Wiley & Sons, New York, 1996, p.74, Ch.2.
22. Bethe, H.A. Theory of diffraction by small holes. *Phys. Rev.* **66**, 163-182 (1944).
23. Ebbesen, T.W., Lezec, H.J., Ghaemi, H.F., Thio, T., Wolff, P.A., Extraordinary optical transmission through sub-wavelength hole arrays, *Nature* **391**, 667-669 (1998).
24. Porto, J.A., Garcia-Vidal, F.J., Pendry, J.B., Transmission resonance on metallic gratings with very narrow slits, *Phys. Rev. Lett.* **83**, 2845-2848 (1999).

25. Ho K. M. et al, Photonic band gap in three-dimensions: new layer-by-layer periodic structure, ***Solid State Communi.*** 89, 413-416 (1994).

Chapter Two

Origin of Absorption Enhancement in a Tungsten Three-dimensional Photonic-Crystal

A three-dimensional metallic photonic-crystal is realized and its absorption measured at infrared wavelengths. The metallic absorption is found to be suppressed in the photonic band-gap regime ($\lambda \sim 8\text{-}20\mu\text{m}$) and enhanced by order-of-magnitude at the photonic band-edge ($\lambda \sim 5.8\mu\text{m}$). The enhancement is attributed to the slower group velocity of light at the photonic band-edge, a longer photon-matter interaction length and a finite intrinsic absorption of tungsten.

Optical absorption is among the most basic photon-matter interaction in nature. Phenomenologically, A. Einstein introduced the so-called "*A*-, *B*- Coefficients" to characterize absorption, spontaneous and stimulated emission processes of a quantized system [1]. Quantum mechanically, *A*-, *B*- coefficients can be described as a summation of dipole-transition matrix-elements over all available photonic density-of-state (DOS) [1]. In a photonic-crystal environment, the photonic DOS may be engineered and a material's absorption rate ($1/\tau_{12}$) be altered. More specifically, in the photonic band-gap regime, photonic DOS vanishes and no light is allowed to either penetrate into or radiate out of a photonic-crystal structure. As light-matter interaction is suppressed, no absorption in the band-gap regime is possible. Another interesting case occurs near and at the photonic band-edge, where the electromagnetic Bloch-wave is still extended throughout the structure, its v_g is near zero and the photonic DOS is greatly increased [2]. In this regime, enhanced light-matter interaction is expected and application of it to enhance absorption [3], laser gain [2-5] and nonlinear effect have all been proposed [3, 4]. It has also been predicated that, at the band-edge, a new photon-atom bound state may occur [6,7]. A photonic crystal thus offers an unique environment for modifying the intrinsic optical interactions inside a material.

In this paper, a tungsten 3D photonic-crystal is realized in the infrared wavelengths and its absorption properties measured and analyzed. The tungsten absorption rate is found to be greatly suppressed in the photonic band gap regime ($\lambda \sim 8\text{-}20\mu\text{m}$) of a tungsten 3D photonic-crystal. More importantly, an order-of-magnitude absorption enhancement is observed at the photonic band-edge. An analysis is performed to understand the underlining mechanisms for absorption enhancement. It is found that the enhancement always occurs at the band-edge, becomes stronger as the sample layer is increased and depends on the material's intrinsic absorption.

The infrared 3D photonic crystals have a diamond crystal symmetry and are fabricated by a layer-stacking design [8]. SEM images of the fabricated 3D silicon and tungsten photonic crystals are shown in Fig. 1(a) and (b), respectively. The 1D rods represent the shortest $\langle 110 \rangle$ chain of atoms in a diamond lattice and are stacked like Lincoln-logs. The rod-to-rod spacing is $a=4.2\mu\text{m}$, the rod width is $w=1.2\mu\text{m}$ and rod height $h \sim 1.5\mu\text{m}$. The stacking sequence is such that every four layers constitute an unit-

cell. The fabrication details for our silicon and tungsten 3D photonic-crystal structures have been described previously [9-11].

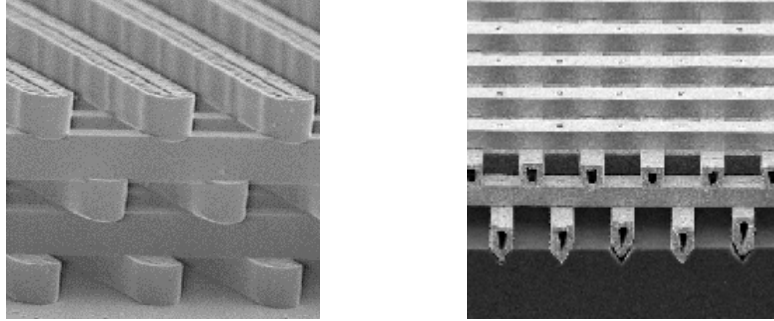


Fig.1

The experimental reflection (R) spectra of the 3D photonic crystals are taken using a standard Fourier-Transform-Infrared-Spectrometer (FTIR) for wavelengths from $\lambda=2-20 \mu\text{m}$. The absorption (A) spectrum is measured using a photo-acoustic method [12]. The photo-acoustic cell is commercially available and can be easily adapted to our FTIR system. To obtain absolute values of R and A, a proper normalization of the sample-signal to a reference-one is necessary. Reflectance from a silver mirror ($R>98\%$ at infrared λ) is used as our reflectance reference. The absorptance-reference is taken from a black-carbon absorber, which has an absorptance of 0.99 for $\lambda=2-20 \mu\text{m}$.

We first study R and A for a 3D silicon photonic crystal. In Fig.2(a), the high reflectance at $\lambda\sim 10-14\mu\text{m}$ indicates the existence of a photonic band-gap. The lower and higher band edges occur at $\lambda\sim 10\mu\text{m}$ and $14\mu\text{m}$, respectively. Despite the intricate reflectance-spectrum, the absorptance-spectrum (blue curve) has no feature and the absorptance is low ($<0.2\%$) for all λ s. This observation is consistent with the fact that silicon is a low-loss dielectric material at $\lambda\sim 1.2$ to $20\mu\text{m}$. In Fig.2(b), we show R and A for a tungsten 3D photonic-crystal sample. Although the data has been reported earlier [9], it is shown here for a comparison purpose. In brief, the reflectance exhibits a large photonic band-gap for $\lambda\sim 8-20\mu\text{m}$, a band-edge at $\lambda\sim 6\mu\text{m}$ and allowed band oscillations for $\lambda<5\mu\text{m}$. More importantly, the absorptance exhibits a pronounced peak at the band-edge of $\lambda\sim 5.8\mu\text{m}$. The peak absorptance of 22% is about one-hundred times larger than that observed ($<0.2\%$) at the band-gap regime ($\lambda>8\mu\text{m}$). The simultaneous suppression and enhancement of absorption at the band-gap and the band-edge, respectively, is important for thermal emission modification. The observation of absorption enhancement only in the metallic 3D photonic-crystal suggests the importance of using metallic materials as well as having the photonic band-edge. The origin of the absorption-rate enhancement is investigated next by theoretically computing R and A using a newly developed Transfer-Matrix method [13]. The method can effectively handle the presence of a complex dielectric function in a metallic 3D photonic-crystal.

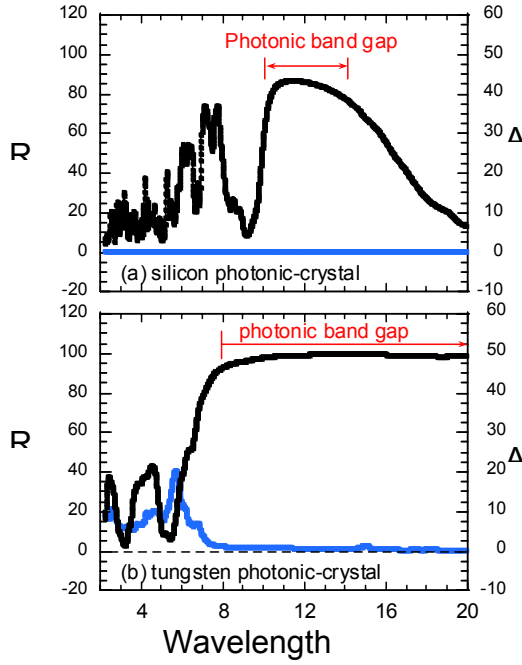


Figure 2

To achieve absorption enhancement in a 3D metallic photonic crystal, three criteria must be satisfied. First, the absorption must occur at the band edge. To verify this, the photonic band-edge position is systematically shifted by increasing the layer thickness, h , from 1.5, 2.0 to 2.4 μm . As it will become clear later that the photonic band-gap dispersion is a strong function of h . In Fig.3, the computed reflectance (black curve) and absorbance (blue curve) spectra for the three cases are shown. The reflectance for the $h=1.5\mu\text{m}$ sample, Fig. 3 (a), shows a band-edge at $\lambda\sim 5.8\mu\text{m}$. At the same λ , an absorption peak of 18% is observed. Both the computed peak-absorbance value and peak-wavelength agree well with the measured ones. For the $h=2\mu\text{m}$ sample, Fig. 3 (b), the first band-edge is shifted to $\lambda\sim 6.6\mu\text{m}$ and the second band-gap at $\lambda\sim 6\mu\text{m}$ has a higher reflectance. Both the first and second absorption peaks occur right at the band-edge of $\lambda\sim 6.6$ and $5\mu\text{m}$, respectively. The absorption at $\lambda\sim 6.6\mu\text{m}$ has a higher absorption amplitude ($\sim 37\%$) and narrower band-width ($\Delta\lambda=0.25\mu\text{m}$) than that for the $h=1.5\mu\text{m}$ sample. As h is further increased to 2.4 μm , the band-edges continue to shift to longer wavelengths and the second band-gap is now well developed. The peak absorption, again, occurs at the band-edge ($\lambda\sim 7.4\mu\text{m}$). The first allowed band is tightly sandwiched between the first and second band-gap, leading to a flatter frequency-wavevector dispersion and a higher DOS. Consequently, the absorption amplitude is further increased to 48% and the band-width narrowed to $\Delta\lambda\sim 0.13\mu\text{m}$. This data shows that absorption-rate, see inset of Fig. 2(b), is preferentially enhanced and always occurs at the photonic band-edges. It is known that group velocity (V_g) of light approaches zero near the band-edge [2]. The

slower moving light thus experiences a longer light-matter interaction time ($\sim 1/V_g$) and is absorbed more strongly. This observation is also consistent with theoretical modeling, which predict that the enhancement is proportional to $1/V_g$ [2,4].

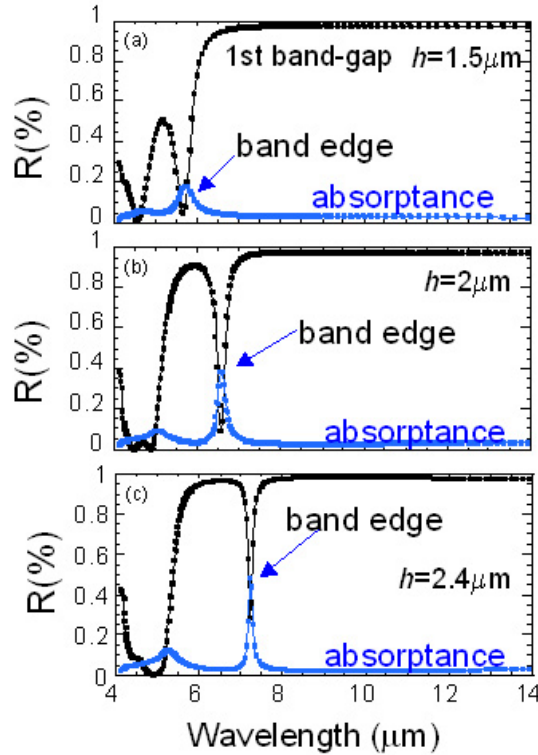


Figure 3

Secondly, the peak absorption-amplitude depends on the number-of-layers (N) of the structure. In contrast, a typical metallic absorption depends on metallic skin-depth of the metal surface layer. The peak absorption-amplitude is computed for samples of different N and is plotted in Fig.4. The peak absorptance (solid dots) is 18% for the $N=4$ sample, or equivalently, one unit-cell. It rises sharply for $4 < N < 8$ and becomes nearly saturated at $\sim 60\%$ for $N > 12$. Meanwhile, the peak λ (open dots) remains essentially unchanged at $\lambda \sim 5.8 \mu\text{m}$ for all N s. The slight increase of the peak- λ for $N > 6$ is due to the fact that the band-edge becomes sharper and moves toward longer- λ for larger N s. For $N < 4$, the structure is less than one unit-cell and neither the band-gap nor the band-edge are well developed. The peak-absorptance saturates at $\sim 60\%$, but not 100%, this is partially caused by a finite reflectance at the air-crystal interface. The functional dependence of the absorptance is exponential-like and is similar to that for an absorbing material with a constant attenuation coefficient. The red curve is a fit to such an exponential function: $A(\lambda \sim 5.8 \mu\text{m}) = b_0 - b_1 \cdot \exp(-\alpha_{\text{eff}} \cdot H)$. Here, b_0 is the saturation value, b_1 is a fitting parameter to take into account the fact that band-gap is well developed only for $N > 4$, $H (=N \cdot h)$ is the total sample thickness and α_{eff} is the effective attenuation constant of light in the tungsten 3D photonic-crystal. The fit is good and the deduced b_0 ,

b_l and α_{eff} are 0.58, 1.9 and $0.26 \mu\text{m}^{-1}$, respectively. The deduced absorption-length ($=1/\alpha_{\text{eff}}$) of $3.8\mu\text{m}$ at $\lambda\sim 5.8\mu\text{m}$ is long compared to the skin-depth (~ 20 nano-meter) of the tungsten material at the same λ . For comparison, this absorption length is compatible to that for a GaAs semiconductor ($1/\alpha_{\text{eff}} \sim 0.8\mu\text{m}$) at $\lambda=0.82\mu\text{m}$. Clearly, light continues to get absorbed as it traverses through the photonic-crystal structure as thick as $21\mu\text{m}$ for the $N=14$ sample. The electro-magnetically excited Bloch-waves can mold its way through the entire photonic-crystal structure, leading to a much longer light-matter interaction length. Thus, the N -dependent absorption amplitude is attributed to the extended nature of the Bloch-waves.

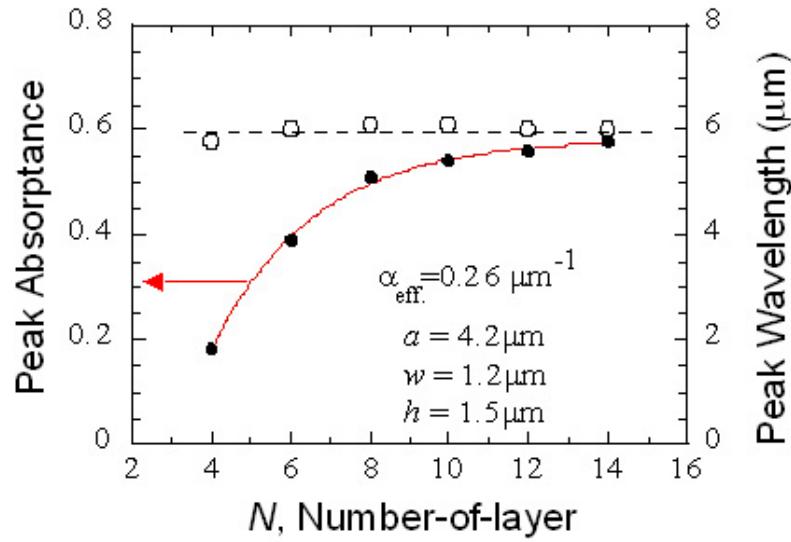


Figure 4

Lastly, the peak absorption must originate from the intrinsic tungsten absorption, or the imaginary part of its dielectric constant, $\epsilon_i(\omega)$. To verify this, absorption spectrum is computed for a series of samples using $\beta\epsilon_i(\omega)$ as a variable. Here, β is a scaling factor ranging from 0% (no intrinsic absorption) to 100% (full intrinsic absorption). In Fig. 5, a summary of the peak absorption amplitude vs β for our tungsten 3D photonic-crystals is shown. The open dots are computed absorptance value for a uniform tungsten film, which increases linearly from 0 to 1.4% as β is varied from 0 to 100%. For the $N=4$ sample, the peak absorption amplitude (solid circles) also scales linearly with β and reaches 18% at the full absorption, $\beta=100\%$. The same scaling behavior has been predicted previously in a calculation for enhanced stimulated emission at the band-edge [4]. This data shows that both the tungsten material absorption and the photonic crystal band-edge absorption have the same origin, which is $\beta\epsilon_i(\omega)$. The effect of photonic band-edge is to enhance the absorption rate from its intrinsic value. Once β is set to zero, no absorption is possible even with the band-edge enhancement effect. This also explains why no absorption is observed for our silicon 3D photonic crystal, as $\epsilon_i(\omega)$ for silicon is low ($< 3 \times 10^{-3}$) in its

transparent regime [14]. For the $N=6$ sample, the absorptance (square dots) increases linearly for $\beta < 75\%$ and starts to slow down at $\beta = 100\%$. For the $N=10$ sample, the absorptance (triangular dots) rises sharply for $\beta < 50\%$ and reaches a saturation value of $\sim 54\%$ at $\beta = 100\%$. One may define an absorption enhancement-factor (η_{abs}) as the ratio of absorption between the tungsten-material and the photonic-crystal at the same β . For $N=10$, the enhancement-factor at the band-edge is as large as $\eta_{\text{abs}} = 100, 70, 50$ and 40 for $\beta = 25, 50, 75$ and 100% , respectively.

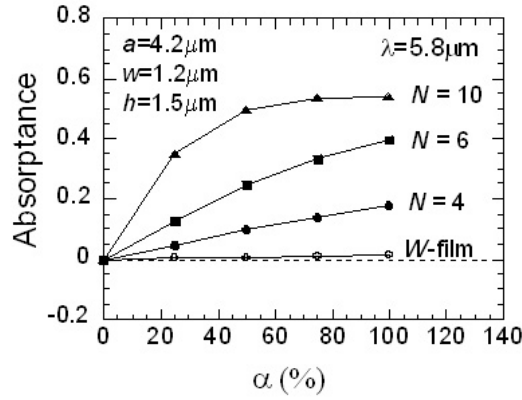


Figure 5

In summary, a 3D metallic photonic-crystal is realized and its absorption measured at infrared wavelengths. The metallic absorption rate is found to be suppressed in the photonic band gap regime ($\lambda \sim 8\text{-}20\mu\text{m}$) and strongly enhanced at the photonic band-edge ($\lambda \sim 6\mu\text{m}$). The peak absorption is shown to originate from the intrinsic tungsten material absorption and is enhanced by the photonic band-edge effect. The enhancement is caused by a longer photon-matter interaction length as compared to the metallic skin depth and the slower group velocity of light at the photonic band-edge.

References

1. R. Loudon, "The quantum theory of light", Ch. 1, p.13-17 and Ch.5, Clarendon Press, Oxford, 1983.
2. J. P. Dowling, M. Scalora, M. J. Bloemer and C. M. Bowden, *J. Appl. Phys.* **75**, 1896-1899 (1994).
3. N. A. R. Bhat and J. E. Sipe, *Phys. Rev. E* **64**, 56604 (2001).
4. K. Sakoda, "Optical properties of photonic crystals", Chapter-5, p.108, Springer-Verlag, New York, 2001.
5. V.I. Koop, B. Fan, H.K. M. Vithana and A.Z. Genack, *Optics Letters* **23**, 1707-1709 (1998).
6. S. John and T. Quang, *Phys. Rev. A* **50**, 1764-1769 (1994).
7. S. John and T. Quang, *Phys. Rev. Lett.* **74**, 3419-3422 (1995).
8. K.M. Ho, C.T. Chan, C. M. Soukoulis, R. Biswas and M. Sigalas, *Solid State Comm.* **89**, 413-416 (1994)
9. S.Y. Lin, J.G. Fleming, D.L. Hetherington, B.K. Smith, R. Biswas, K.M. Ho, M.M. Sigalas, W. Zubrzycki, S.R. Kurtz and J. Bur, *Nature* **394**, 252-253 (1998).
10. J. G. Fleming, S.Y. Lin, I. El-Kady, R. Biswas and K. M. Ho, *Nature* **417**, 52-55 (2002).
11. S.Y. Lin and J. G. Fleming, *Optics Letters* **24**, 49-51 (1999).
12. McClelland, J.F., Jones, R.W., Lou, S., and Seaverson, L.M., A Practical guide to FTIR photoacoustic spectroscopy, in *Practical sampling techniques for infrared analysis*, P.B. Coleman, Ed. (CRC Press, Boca Raton, Florida, 1993), Chapter 5.
13. Z. Y. Li, I. El-Kady, K. M. Ho, S. Y. Lin and J. G. Fleming, Submitted to *Phys. Rev. Letts.*
14. "Handbook of Optical Constants of Solids", Edited by Edward D. Palik, p.555-568. Academic Press, London, 1998.

Chapter Three

SELECTIVE EMITTERS USING PHOTONIC CRYSTALS FOR THERMOPHOTOVOLTAIC ENERGY CONVERSION

ABSTRACT

Photonic crystals use a periodic modulation of the refractive index to alter the photonic density of states. The photonic density of states is an important parameter in many phenomena involving radiation-matter interactions – including thermal emission of radiation. Hence, a photonic crystal can be used to engineer the emissivity of an emitter for thermophotovoltaic (TPV) generators to match the spectral response of the photovoltaic cell. The use of photonic crystals in TPV is described. A three-dimensional photonic crystal in tungsten is realized that exhibits an exceptionally large photonic bandgap and attenuation factor. The photonic crystal is shown to have promise for radiant energy conversion applications like TPV energy conversion.

INTRODUCTION

Thermophotovoltaic (TPV) energy conversion converts the radiant energy of a high-temperature body (“emitter”) directly into electricity using a photovoltaic cell. TPV has a number of attractive features, including: fuel versatility (nuclear, fossil, solar, etc.), quiet operation, low maintenance, low emissions, light weight, high power density, modularity, and cogeneration of heat and power. TPV could potentially be used for distributed power, automotive, military, and other applications wherever fuel cells, microturbines, or cogeneration are presently being considered if the TPV efficiencies could be raised to around 30%. While the concept is very old, TPV is experiencing renewed interest due to recent advances in low-bandgap photovoltaic (PV) cells.^{i,ii} Low-bandgap photovoltaic cells are required to work with emitters at manageable temperatures (1300 to 1800K).

The parameters that affect TPV system performance has been examined by many authors.¹ A TPV system efficiency is the product of the fuel-to-radiation efficiency and of the radiation-to-electricity efficiency. The fuel-to-radiation efficiency is dependent upon the application, fuel source, and other engineering details. This paper will examine the second factor of radiation-to-electricity efficiency, since this factor is common to all TPV

generators and we wish to examine new approaches to enhancing this component. The radiation-to-electricity conversion efficiency will be referred to as the “TPV efficiency”.

The emitter temperature is mostly determined by the fuel source. The spectrum from the emitter is determined by the emissivity of the emitter and by the emitter temperature. The TPV efficiency for a given spectrum varies as a function of the PV cell bandgap; the optimum bandgap is wider (smaller) for higher (lower) temperature emitters.

Given a selection of operating temperature and PV cell, the efficiency of a TPV system is determined by the control of the radiation spectrum on the PV cell. In particular, the efficiency of the PV cell is improved by matching the spectrum of the radiation to the spectral response of the photovoltaic cell. For example, photovoltaic cells can have energy-conversion efficiencies over 50% if illuminated with monochromatic light near the bandgap.ⁱⁱⁱ Spectral control can be achieved by either controlling the spectrum of the emitted radiation (“selective emitter”) or by using spectral filters to return unwanted radiation to the emitter. Achieving high efficiencies requires very high performance in terms of the spectral selectivity or reflectivity, bandwidth, and the angular distribution with either a selective emitter or a spectral filter.^{iv}

Recently, the control of spectral emissivity by physically structuring the emitter has been examined by several researchers.^{v,vi} This is a new and powerful approach to controlling emissivity that can use well-established materials and tools from the microelectronics and thin-film industries.

We describe the use of photonic crystals as a selective emitter for TPV energy conversion. We first describe the general properties of photonic crystals and how they can be used to tune emissivity. Next, we present some preliminary experimental results using photonic crystals constructed using tungsten. Next, we model the performance of TPV systems using photonic-crystal selective emitters. Finally, we compare the prospects of photonic crystals for enhancing TPV energy conversion efficiency compared to other selective-emitter approaches.

PHOTONIC CRYSTALS and THERMAL EMISSION

Photonic crystals are structured materials where the refractive index is modulated in one, two, or three dimensions.^{vii} The modulation of the refractive index alters the photonic density-of-states spectrum. A photonic state is essentially an allowed optical mode in the structure. Many properties involving the interaction of radiation and materials, such as spontaneous emission and thermal emission of radiation, were once thought of as intrinsic properties of the material. However, these properties are, in fact, a function of the photonic density of states through Fermi’s Golden Rule (Eq. 1).^{viii,ix}

$$p_{i \rightarrow f}(\omega_k) \propto \rho(\omega_k) \cdot \left| \langle i | \boldsymbol{\mu} \cdot \mathbf{E}_k(\omega_k) | f \rangle \right|^2 \quad \text{Eq. 1.}$$

This equation represents the probability of a radiative transition from an initial state i to a final state f for optical mode ω_k . The term in the brackets is the quantum mechanical

matrix element associated with the radiative transition, which is the product of the electric dipole moment μ and electric field E_k for optical mode ω_k . The matrix element is multiplied by the density of optical modes at ω_k – i.e., the photonic density of states $\rho(\omega_k)$ —to get the transition rate. Hence, modification of the photonic density of states can directly modify the radiative transition rate.

The emission of thermal radiation is more commonly described with classical mechanics through the definition of emissivity.

$$I(\lambda, T) = \varepsilon(\lambda) \cdot I_{BB}(\lambda, T)$$

$$I_{BB}(\lambda, T) = \frac{2\pi^5 k^4}{15} \frac{1}{\lambda^5} \frac{1}{e^{\lambda k T} - 1} \quad \text{Eq. 2}$$

Eq. 2 states that the thermal radiation from a graybody is equal to the emissivity $\varepsilon(\lambda)$ multiplied by the thermal radiation from a blackbody $I_{BB}(\lambda)$ (Planck’s Law). For purely thermal emission, it can be shown that the emissivity is equal to absorptivity (Kirchoff’s Law), which provides a convenient method for calculating and measuring emissivity.^x The emissivity is less than unity since no radiator can emit thermal radiation greater than a blackbody. In general, the emissivity could also be a function of angle. The quantum and classical descriptions are, of course, fully equivalent.⁹

The significance of this discussion is that the radiation-matter interaction is subject to engineering through physical structuring of the material(s) into a photonic crystal. It is even possible to design structures where there are no photonic states for a specific frequency range; i.e., a *photonic bandgap*. Such structures are said to exhibit a *full* photonic bandgap if there are no photonic states in any direction and for any polarization. (The *bandgap* terminology is borrowed from solid-state physics where crystal symmetry leads to a similar gap in the density of states for electrons.) As implied by Eq. 1 and 2, the radiative transition probability and the spectral emissivity are zero within a *full* photonic bandgap. Photonic crystals therefore provide the ultimate control of emissivity since these structures can achieve a true photonic bandgap.

The important parameters of a photonic crystal include the crystal symmetry and lattice constant, which determine the bandgap of the photonic crystal, and the refractive index contrast, which determines the magnitude and bandwidth of the photonic bandgap. Three-dimensional photonic crystals can exhibit a full photonic bandgap. One- and two-dimensional photonic crystals generally do not exhibit a *full* photonic bandgap; rather, they generally exhibit a photonic bandgap only for a narrow range of angles and/or for specific polarizations.

We (S-Y. Lin and J. G. Fleming) have previously demonstrated the alteration of thermal emission by a three-dimensional photonic crystal.^{xi} We fabricated and measured the thermal emission of a three-dimensional photonic crystal in polycrystalline silicon.

Silicon behaves optically like a dielectric in the infrared. The thermal emission was suppressed in the photonic bandgap and was enhanced in the photonic passband, which matched the expected alteration of the photonic density of states in the silicon photonic crystal. Hence, the issue is developing and demonstrating the potential of a photonic crystal for enhancing TPV energy conversion.

EXPERIMENT

Practical TPV energy conversion systems require high emitter temperatures, e.g., around 1800K, to obtain high efficiencies and power densities. The high temperatures require refractory materials for the emitter. Tungsten is widely used in such refractory applications as incandescent light bulbs because the material is easily drawn into thin filaments and can handle the high temperatures. Metals also offer the advantage, compared to dielectrics, of a very large refractive index contrast that enhances the effects of photonic structures. In particular, a large photonic bandgap is needed to suppress the long-wavelength infrared emission of a blackbody. Finally, tungsten is advantageous since it can be easily deposited and patterned using commonly available tools from the microelectronics industry.

We developed a process for producing three-dimensional tungsten photonic crystals using the basic process used to fabricate our three-dimensional polycrystalline-silicon photonic crystals. The polycrystalline-silicon photonic crystal consists of a stack of layers with rods (Fig. 2). Each layer of rods is produced using common processes from the microelectronics industry -- oxide deposition, patterning to open a trench, polycrystalline-silicon deposition in the trench, and chemical-mechanical polishing to planarize the surface. Layers of rods are sequentially fabricated and the oxide is removed at the end. The result is a face-centered cubic crystal.^{xii} The tungsten crystal is obtained by first fabricating a photonic crystal in polycrystalline-silicon in a silicon dioxide matrix with the aforementioned fabrication sequence. The polysilicon is then removed with a chemical etch, which leaves a silicon-dioxide mold of the photonic crystal. Tungsten is deposited into this mold with chemical vapor deposition, and then the silicon dioxide mold is removed with a chemical etch.^{xiii}

The photonic crystals were characterized via reflectance, transmittance, and absorptance measurements using a Fourier-transform infrared measurement system (FTIR) from 1.5 to 25 μm (Fig. 3 and 4). The metallic photonic crystal exhibited an enormous bandgap (around 8 to over 20 μm) and attenuation factor (30 dB per unit cell at 12 μm), as well as a transmittance and absorptance band near the edge of the photonic bandgap. The extremely large photonic bandgap and attenuation factor are due to the very large refractive index contrast using a metallic photonic crystal, while the absorption band is due to the unusual electromagnetic behavior associated with metallic photonic crystals. The fabrication, characterization, and, in particular, the unusual electromagnetic modes in metallic photonic crystals are described elsewhere.¹³ We have also directly measured the emission of a tungsten photonic crystal that was heated electrically, and confirmed that the emission spectra matched the absorption spectra as expected from Eq. 2.^{xiv} It should also be noted that modeling calculations of the tungsten photonic crystal reproduce the

spectral features well and, for example, predict that the absorptance in Fig. 4 can be increased by adding more layers to the photonic crystal.

RESULTS and TPV MODEL

The present tungsten photonic crystal has a cutoff wavelength of around 8 μm . As is well known in photonic crystal physics, the cutoff wavelength can be moved to shorter wavelengths by using a smaller lattice constant for the photonic crystal. In order to compare the performance of a tungsten photonic crystal designed for TPV applications with other selective emitter approaches, we projected the spectral emissivity of a tungsten photonic crystal where the cutoff wavelength is moved to around 1.7 μm – which is the appropriate cutoff wavelength to use with a GaSb photovoltaic cell (E_g of 0.72 eV). This was achieved by: (1) equating the absorptivity with emissivity (Fig. 4), and (2) dividing the wavelength scale by 3.4. This scaling corresponds to a tungsten photonic crystal with a lattice constant of 1.2 μm , which is compatible with current fabrication technology. This scaling procedure was adopted since, as previously mentioned, the modal dispersion relation in photonic crystals scales as the wavelength divided by the lattice constant.

We constructed a simple one-dimensional model of TPV energy conversion (Appendix). The purpose of the model is to compare the potential performance of a more optimal tungsten photonic crystal with other selective-emitter approaches that have been described in the literature. This model therefore does not include a model of the process to heat the emitter. The model also does not try to provide a realistic estimate of total system conversion efficiency since it neglects radiative and convective losses. Rather, the model provides performance trends as a function of different spectral properties in the TPV system.

The model for the GaSb photovoltaic cell and the TPV system is similar to the model described by Zenker *et al.*² We estimated the TPV efficiency (photovoltaic cell output divided by net radiant flux) with our scaled tungsten photonic crystal, with a microstructured tungsten emitter³, with an erbia/yttria selective emitter, and with an ideal blackbody.

Our TPV system calculations found a much higher projected radiation-to-electricity conversion efficiency for the photonic crystal compared to the other selective-emitter approaches (Table 1). Note that the higher conversion efficiency was achieved at the expense of a much reduced power density. As previously noted, modeling calculations show that the absorptivity (and therefore emissivity) can be increased further by increasing the number of layers – which would improve the power density without changing the energy conversion efficiency. Power density is an issue with any selective emitter and affects the economics of the TPV system.

CONCLUSION

Photonic crystals offer a completely new and powerful method for modifying the spectral emissivity of thermal emitters. Photonic crystals provide the ultimate control of emissivity since they can achieve a true photonic bandgap where there is a complete absence of photonic states. Spectrally selective emitters based on photonic crystals could

be used to substantially enhance the efficiency of thermophotovoltaic energy converters, incandescent lamps, or any other application using high-temperature radiators.

APPENDIX: DESCRIPTION OF TPV MODEL

A simple one-dimensional model was constructed to model the radiative fluxes in a TPV energy conversion system. Such a model neglects losses of radiation and heat via conduction from the ends of the TPV chamber. The quantities of primary interest include the net radiated power density Q_r , the maximum electrical power density P_{\max} , and the maximum conversion efficiency η_{\max} . These quantities are given by:

$$\eta_{\max} \equiv \frac{P_{\max}}{Q_r} \quad (\text{A1})$$

$$P_{\max} \equiv [JV]_{\max} \quad (\text{A2})$$

where J and V are the current density and voltage of the PV cell.

The set of planar optical elements that describe a TPV system include the emitter, an optional optical filter, a cell “window” (optical coating on the front surface of the PV cell), a PV cell, and a reflecting back plane. This model with the spectral fluxes is represented schematically as:

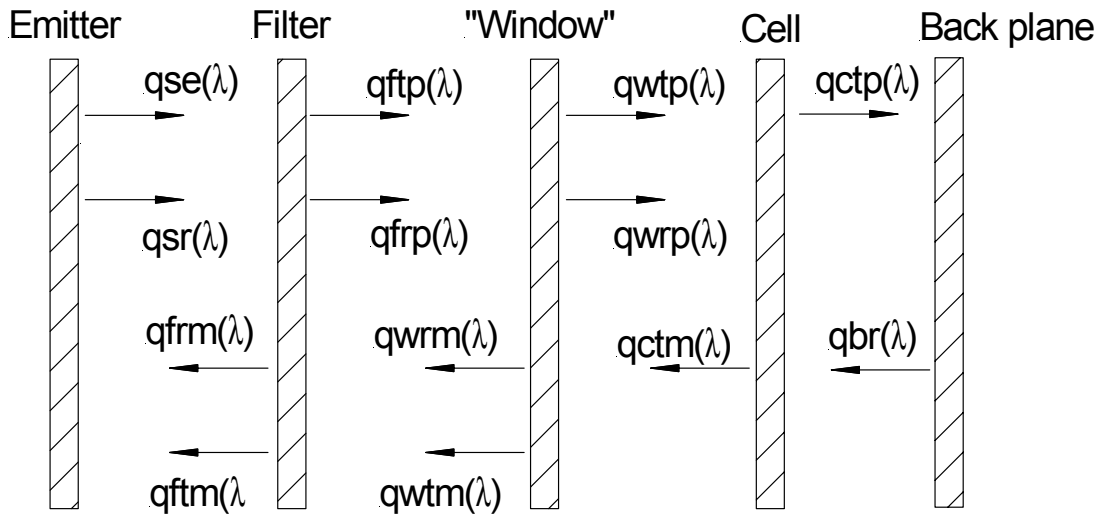


Figure A1. An illustration of radiative fluxes in a simple one-dimensional model of TPV energy conversion that includes only spectral effects.

The relevant optical properties (absorptivity A , transmissivity T , reflectivity R , and emissivity ϵ) for each planar optical element are given by:

Emitter: $\epsilon_s(\lambda)$ specified, $T_s(\lambda) = 0$, $A_s(\lambda) = \epsilon_s(\lambda)$, $R_s(\lambda) = 1 - \epsilon_s(\lambda)$
 Filter: $T_f(\lambda)$ and $A_f(\lambda)$ specified, $R_f(\lambda) = 1 - T_f(\lambda) - A_f(\lambda)$
 Window: $R_w(\lambda)$ specified, $A_w(\lambda) = 0$, $T_w(\lambda) = 1 - R_w(\lambda)$
 Cell: $A_c(\lambda)$ specified, $R_c(\lambda) = 0$, $T_c(\lambda) = 1 - A_c(\lambda)$
 Back plane: $R_b(\lambda) = 1$

The spectral fluxes (q in W/m^2) are given by:

$$q_{se}(\lambda) = \frac{2\pi hc^2 \epsilon_s(\lambda)}{\lambda^5 (e^{\frac{hc}{kT\lambda}} - 1)} \quad (\text{A3})$$

$$q_{frm}(\lambda) = (q_{se}(\lambda) + q_{sr}(\lambda))R_f(\lambda) \quad (\text{A4})$$

$$q_{sr}(\lambda) = (q_{frm}(\lambda) + q_{fim}(\lambda))R_s(\lambda) \quad (\text{A5})$$

$$q_{fim}(\lambda) = (q_{wrm}(\lambda) + q_{wtm}(\lambda))T_f(\lambda) \quad (\text{A6})$$

$$q_{ftp}(\lambda) = (q_{se}(\lambda) + q_{sr}(\lambda))T_f(\lambda) \quad (\text{A7})$$

$$q_{frp}(\lambda) = (q_{wrm}(\lambda) + q_{wtm}(\lambda))R_f(\lambda) \quad (\text{A8})$$

$$q_{wtm}(\lambda) = q_{ctm}(\lambda)T_w(\lambda) \quad (\text{A9})$$

$$q_{wrm}(\lambda) = (q_{frp}(\lambda) + q_{ftp}(\lambda))R_w(\lambda) \quad (\text{A10})$$

$$q_{wtp}(\lambda) = (q_{frp}(\lambda) + q_{ftp}(\lambda))T_w(\lambda) \quad (\text{A11})$$

$$q_{wrp}(\lambda) = q_{ctm}(\lambda)R_w(\lambda) \quad (\text{A12})$$

$$q_{ctp}(\lambda) = (q_{wtp}(\lambda) + q_{wrp}(\lambda))T_c(\lambda) \quad (\text{A13})$$

$$q_{br}(\lambda) = q_{ctp}(\lambda)R_b(\lambda) \quad (\text{A14})$$

$$q_{ctm}(\lambda) = q_{br}(\lambda)T_c(\lambda) \quad (\text{A15})$$

λ is the wavelength, k is Boltzman's constant, h is Plank's constant, c is the speed of light, and T is the temperature of the emitter. The subscripts on q refer to the optical element (e.g., s is source, f is filter, etc.), source of the flux (e is emitter, t is transmitted, r is reflected, etc.), and direction of propagation (p is towards PV cell and m is towards emitter).

The net flux radiated from the source Q_r is:

$$Q_r = \int_0^{\infty} \{q_{se}(\lambda) - A_s(\lambda)[q_{fm}(\lambda) + q_{im}(\lambda)]\}d\lambda \quad (A16)$$

The current density and cell voltage depend on the cell model. Following Zenker *et al.*, we assume that the PV cell is totally absorbing for wavelengths less than bandgap wavelength λ_g . The short-circuit current density is then given by:

$$J_{sc} = \int_0^{\lambda_g} \{q_{wtp}(\lambda)\}R(\lambda)d\lambda \quad (A16)$$

where $R(\lambda)$ is the spectral response of the PV cell,

$$R(\lambda) = \frac{\lambda QE(\lambda)e}{hc} \text{ (A/W)}. \quad (A17)$$

Zenker *et al* used a sophisticated device model to model the GaSb cell performance. We used a simple lumped-parameter model of PV cells as described by Coutts¹, with the value of the lumped parameters adjusted to match the results provided by Zenker *et al.* The model equations were programmed into a commercial mathematical software package (MathCadTM). Excellent agreement was obtained between the calculations presented in Zenker and with our model.^{xv}

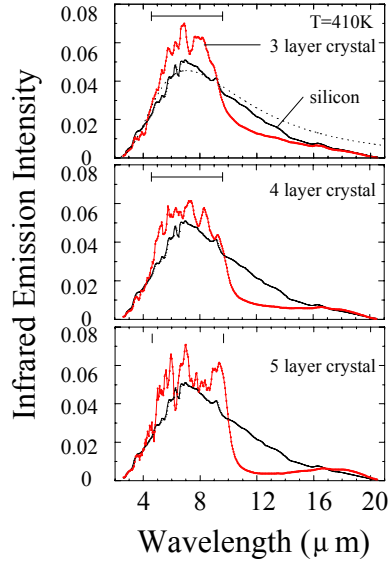


Figure 1. **Thermal emission from a 3D photonic crystal constructed of polysilicon at 410K. The photonic crystal has a lattice spacing of 4.2 μm and diamond crystal symmetry. The number of layers refers to the number of layers in the photonic crystal. The suppressed thermal emission between 10 and 16 μm is due to the *full* photonic bandgap of the 3D photonic crystal.¹¹**

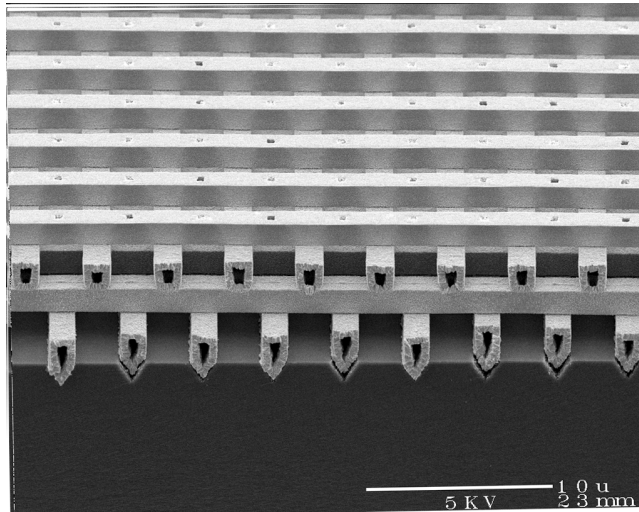


Figure 2. SEM photomicrograph of cross section of a 4-layer 3-dimensional tungsten photonic crystal. The photonic crystal has a lattice spacing of $4.2 \mu\text{m}$ and a diamond crystal symmetry. The tungsten rods are hollow due to poor step coverage of the tungsten CVD step.

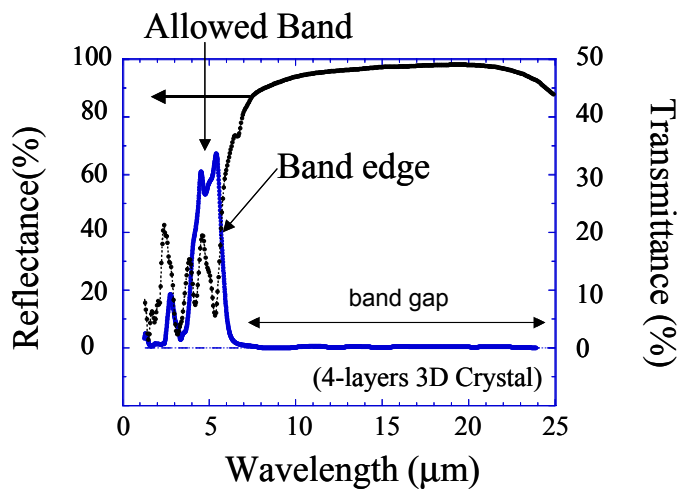


Figure 3. Spectral reflectance and transmittance of 4-layer 3-dimensional tungsten photonic crystal.

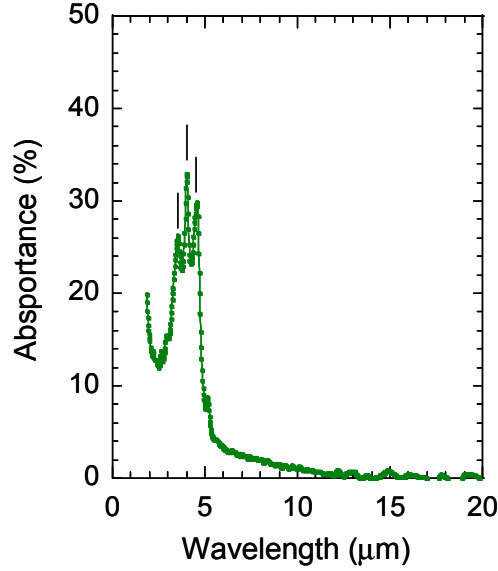


Figure 4. Spectral absorptance of 4-layer 3-dimensional tungsten photonic crystal.

Table 1. Results of TPV calculations using various emitters. The model used an 1800K radiator and GaSb photovoltaic cell at 300K. The emissivity of the microstructured tungsten emitter was taken from Heinzl *et al.*⁵, and the emissivity of the erbia/yttria emitter was taken from Crowley *et al.*^{xvi}

Emitter	Radiant flux (W/cm ²)	Electric power (W/cm ²)	Eff. (%)
Blackbody	56.9	7.2	12.6
Tungsten Photonic crystal	5.4	1.4	26.2
Microstructured Tungsten	19.6	4.4	22.4
Erbia/yttria	16.6	2.6	15.5

REFERENCES

- ¹ T.J. Coutts, "A review of progress in thermophotovoltaic generation of electricity," *Renewable and Sustainable Energy Reviews* **3**, 77-184 (1999).
- ² O.V. Sulima and A.W. Bett, "Fabrication and simulation of GaSb thermophotovoltaic cells," *Solar Energy Mat. & Solar Cells* **66**, 533 (2001); and R.M. Biefeld, *et al.*, "The growth and characterization of GaInAsSb and AlGaAsSb on GaSb by metal-organic chemical vapor deposition," *J. Crystal Growth* **225**, 384 (2001).
- ³ M.A. Green, "Limiting photovoltaic monochromatic light conversion efficiency," *Progress in Photovoltaics* **9**, 287 (2001).
- ⁴ Matthias Zenker, *et al.*, "Efficiency and power density potential of combustion-driven thermophotovoltaic systems using GaSb photovoltaic cells," *IEEE Trans. Elect. Dev.* **48**, 367 (2001).
- ⁵ A. Heinzl, *et al.*, "Microstructured Tungsten Surfaces as Selective Emitters", in "Thermophotovoltaic Generation of Electricity: Fourth NREL Conference", T. J. Coutts *et al.*, ed., AIP, 1999; and A. Heinzl, *et al.*, "Radiation filters and emitters for the NIR based on periodically structured metal surfaces," *J. Modern Optics* **47**, 2399 (2000).
- ⁶ S. Maruyama, *et al.*, "Thermal radiation from two-dimensionally confined modes in microcavities," *Appl. Phys. Lett.* **79**, 1393 (2001).
- ⁷ John D. Joannopoulos, Robert D. Meade, and Joshua N. Winn, **Photonic Crystals: Molding the Flow of Light** (Princeton University Press, 1995).
- ⁸ Eli Yablanovitch, "Inhibited spontaneous emission in solid-state physics and electronics," *Phys. Rev. Lett.* **20**, 2059 (1987).
- ⁹ C.M. Cornelius and J.P. Dowling, "Modification of Planck blackbody radiation by photonic band-gap structures," *Phys. Rev.* **A59**, 4736 (1999).
- ¹⁰ R. Siegal and J.R. Howell, **Thermal Radiation Heat Transfer**, 3rd ed., 1992.

¹¹ Shawn-yu Lin, *et al.*, “Enhancement and suppression of thermal emission by a three-dimensional photonic crystal,” *Phys. Rev.* **B62**, R2243 (2000).

¹² Shawn-yu Lin, *et al.*, “A three-dimensional photonic crystal in the infrared wavelengths,” *Nature* **394**, 252 (1998).

¹³ J.G. Fleming, *et al.*, “All metallic three-dimensional photonic crystals with a large infrared bandgap,” *Nature* **417**, 52 (2002).

¹⁴ S-Y. Lin and J.G. Fleming, to be published.

¹⁵¹ James B. Moreno, “Planar TPV model with multiple optical elements, full spectral detail, and empirical cell behavior,” Sandia National Laboratories internal memo, April 24, 2001.

¹⁶ C. J. Crowley, *et al.*, “Thermal Spray Approach for TPV Emitters”, in “Thermophotovoltaic Generation of Electricity: Fourth NREL Conference

Publication Lists

1. “All-metallic 3D photonic crystals for photon energy recycling”, *Nature* **417**, 52-55 (2002).
2. “Origin of absorption enhancement in a tungsten photonic”, submitted *J. of Optical Society of America*, **July 2002**.
3. “Selective emitters using photonic crystals for thermal voltaic energy conversion”, *to be submitted*.

Distribution

1	MS 9018	Central Technical Files, 8945-1
2	MS 0899	Technical Library, 9616
1	MS 0612	Review and Approval Desk, 9612, for DOE/OSTI
1	MS 0188	Technology Transfer, 1321
1	MS 0188	D. Chavez, LDRD Office, 1030
2	MS 0603	S.Y. Lin, 1743
2	MS 1080	J.G. Fleming, 1749
2	MS 0752	J Gee, 6216
2	MS 0752	J Moreno, 6216
